Investigation to the ultrastructural changes in SJL/J mice following antioxidant supplementation

6.1 INTRODUCTION

The assessment of muscle on the ultrastructural level has, according to Cenacchi and co-workers, 2007, a strategic position in improving the diagnostic accuracy of the histopathology not revealed by light microscopy. It gives insight into the pathophysiologic mechanisms and can guide molecular genetic analysis (Cenacchi *et al*., 2007). For effective analysis on the ultrastructural level, it is important to have a clear picture of the ultrastructural anatomy of mammalian skeletal muscle and the way the integrated components cooperate to produce function. It is moreover essential to have a sound understanding of the structure and functioning of healthy muscle in order to link alterations at the ultrastructural level to the pathology in a diagnostic approach. Therefore an overview of muscle ultrastructure and function are presented.

6.1.1 OVERVIEW OF SKELETAL MUSCLE ULTRASTRUCTURE

Myofibrils are the contractile structures of a muscle fiber (Figure 6.1). A sarcomere extends between two dark lines called the Z-discs. There are two types of protein filaments: the thick filaments, which are made up of myosin, and the thin filaments, which are made up of actin. The I-band is light coloured because it contains only actin filaments attached to a Z-line. The darker regions of the A-band contain overlapping actin and myosin filaments, while only myosin filaments are present in the H-zone (Mader, 2001). Surrounding the fibrils and accumulated near the nuclei are the remaining cytoplasmic components of the fiber, collectively called the sarcoplasm (Kelly *et al*., 1984). Each muscle contains a thousand or more myofibrils that occupy most of the intracellular volume, leaving little space for the sarcoplasm (Silverthorn, 2004).

Myofibrils

Each myofibril is composed of several types of proteins: the contractile proteins, myosin and actin, the regulatory proteins, tropomyosin and troponin, and the giant accessory proteins titin and nebulin (Silverthorn, 2004). Myosin is the protein that makes up the thick filaments of the myofibril. Each myosin molecule is composed of two heavy protein chains that intertwine to form a long coiled tail and a pair of heads. Two lightweight protein chains are associated with the heavy chain of each head (Silverthorn, 2004). In skeletal muscle about 250 myosin molecules join to create a thick

filament. The thick filament is arranged so that the myosin heads are clustered at the ends, and the central region of the filament forms a bundle of myosin tail.

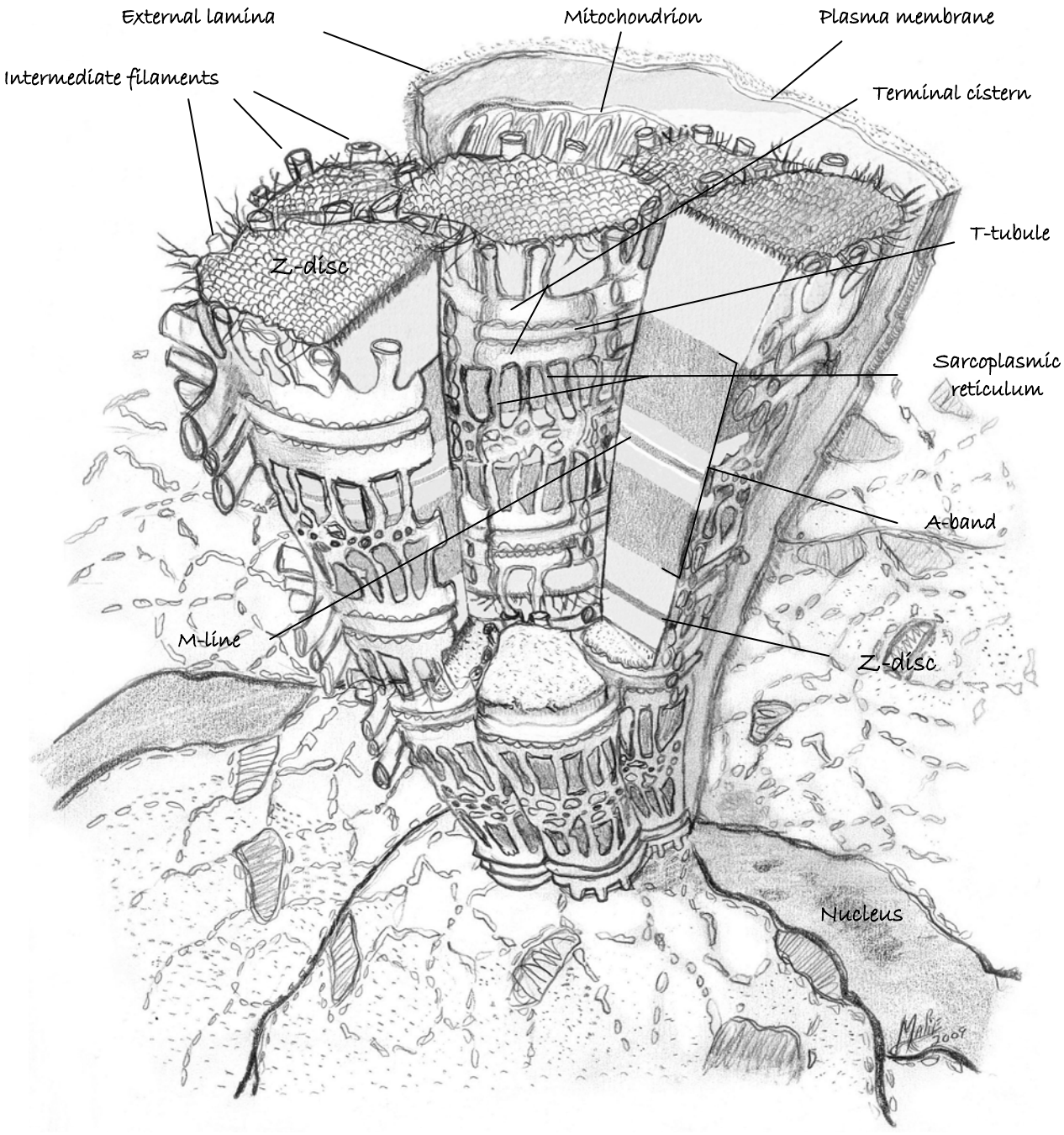

Figure 6.1: Schematic representation of the components in and around skeletal muscle myofibrils on an ultrastructural level. (Adapted from Kelly *et al*., 1984)

The rodlike portion of the thick filament is stiff, but the protruding myosin heads have an elastic hinge region where the heads join the rods. The hinge region allows the heads to swivel around their

point of attachment (Silverthorn, 2004). Actin is the protein that makes up the thin filaments of the muscle fiber. One actin molecule is a globular protein (G-actin). Multiple globular actin molecules polymerize to form long chains or filaments (F-actin). In skeletal muscle, two F-actin polymers twist together like a double strand of beads, creating the thin filaments of the myofibril (Silverthorn, 2004).

Myofibrils range from 1 to 2µm in diameter, but may be as small as 0.2µm (Kelly *et al*., 1984). In a cross section of a fiber the myofibrils are usually visible as punctuated densities with individual size and shape, separated from each other by narrow clear sarcoplasmic regions (Kelly *et al*., 1984). The arrangement of thick and thin filaments in a myofibril creates a repeating pattern of alternating light and dark bands (Silverthorn, 2004). One repeat of the pattern forms the sarcomere, which is the fundamental structural and functional unit of contraction in skeletal muscle (Kelly *et al*., 1984).

Sarcomeres

Each sarcomere is composed of smaller segments or 'bands' recognized by distinctive refractive differences (Kelly *et al*., 1984). The broad, darkly stained band is doubly reflective or anisotropic under polarized light, and is therefore known as the A-band (Kelly *et al*., 1984). At the outer edges of the A band, the thick and thin filaments overlap. The center of the A-band is occupied by thick filaments only (Silverthorn, 2004). The lightly stained band is relatively monorefringent or isotropic and is known as the I-band. Each of these bands is bisected by a narrow zone. It is dense in the I-bands and designated the Z-line or disc (from the German *Zwishenscheibe*, between disc) (Kelly *et al*., 1984). The portion of fibril between two successive Z-discs is a sarcomere. Its length in relaxed mammalian muscle is 2 to 3µm. It may be stretched to a greater length, and in greatly contracted fibers it may be reduced to about 1µm (Kelly *et al*., 1984). These zigzag structures are made up of proteins that serve as the attachment site for thin filaments (Silverthorn, 2004). The zone bisecting the A-band is pale and designated H (both from the German for light, *helles*, and the name of the discoverer, Hensen) (Kelly *et al*., 1984). The attachment site for the thick filaments, equivalent to the Z-disc for the thin filaments, is the M-line (from the German word for middle, *mittel*). An M-line divides one A-band in half (Silverthorn, 2004).

The sarcoplasm

The sarcoplasm is a complex assemblage of organelles which provides special structural and energetic support for the contractile apparatus, while also serving the general metabolic requirements of the living cellular system (Kelly *et al*., 1984). It includes an elaborate endoplasmic reticulum. This sarcoplasmic reticulum is a supportive framework of intermediate and finer filaments, microtubules, a golgi complex, variable amounts of mitochondria, few ribosomes,

glycogen and occasional lipid droplets (Kelly *et al*., 1984). The mitochondria of the muscle cell are found beneath the sarcolemma, around the nuclei, and in the sarcoplasm between the myofibrils. In this location, they are generally aligned with their long axis parallel to the direction of the myofibril. They may also be found encircling the myofibril transversely, particularly in the region overlying the Z-disc (Kelly *et al*., 1984).

The sarcoplasmic reticulum can be seen in electron micrographs as a network of cisterns or membranous tubules which run between and around the myofibrils (Kelly *et al*., 1984). It is an agranular reticulum because the relatively few ribosomes present are scattered through the cytoplasm and are not aligned on the membranes (Kelly *et al*., 1984). The cisterns run chiefly parallel to the myofibrils. Lateral anastomoses between the parallel or longitudinal cisterns form a perforated collar around the myofibrils at the level of the H-zone. In the vicinity of the I-band or Z-disc, the sarcoplasmic reticulum is expanded into terminal cisterns. These tend to be arranged into pairs which flank another, single membranous passage, the transverse tubule (T tubule) (Kelly *et al*., 1984).

T tubule system

The transverse tubular system or T system consists of numerous tubular invaginations of the plasma membrane (Ross *et al*., 2003). Each T tubule and its closely apposed two terminal cisterns constitute a triad. T tubules penetrate to all levels of the muscle fiber and show a triadic organization, accompanying terminal cisterns at the level of each A-I junction in mammalian skeletal muscle. T tubules provide two sets of tubules and terminal cisterns per sarcomere (Kelly *et al*., 1984; Ross *et al*., 2003). Their walls provide narrow tubular extensions of the cell membrane into the depths of the muscle fiber. Here they form complex membrane-to-membrane junctions with the membranes of terminal cisterns, within each triad. These are termed the triadic junctions or triadic couplings (Kelly *et al*., 1984). They contain voltage sensor proteins, depolarization-sensitive transmembrane channels, which are activated when the plasma membrane depolarizes. Conformational changes of these proteins affect gated Ca^{2+}-release channels located in the adjacent plasma membrane of the terminal cisternae (Ross *et al*., 2003). T tubules afford coordinated activity of all myofibrils as they serve for rapid transmission of impulses from the exterior to the deepest regions of the cell (Kelly *et al*., 1984).

Why an ultrastructural investigation?

Cenacchi and co-workers, 2007, described electron microscopy (EM) as an interesting tool for studying muscle pathologies. As a diagnostic tool, the main indication for EM is myopathies with

autophagic vacuoles, as it provides an understanding of pathological mechanisms of various muscular diseases and can even guide genetic analysis (Cenacchi *et al*., 2007). This chapter followed a qualitative investigation to the ultrastructure of SJL/J mice supplemented with the antioxidants CoQ10 and resveratrol for 90 days. Results are compared to that of the unaffected SWR/J strain as well as to that of 14 and 27 week-old SJL/J mice who received no antioxidant therapy. This chapter further elaborates on the light microscopic findings of chapter 5, as it focuses on the specific and non-specific ultrastructural changes that exemplify the dystrophic alterations in muscle tissue of the SJL/J mouse model. Electron micrographs were generated using transmission and scanning electron microscopy (TEM and SEM).

6.2 Materials and Methods

For ultrastructural analyses, quadriceps muscle samples (of all groups) were collected at termination. A small piece (± 1.5 x 2mm) of muscle tissue was dissected out from the belly area of the quadriceps muscles. Tissue samples were immediately fixed in 2.5% glutaraldehyde (SPI Supplies, West Chester, PA) and 2.5% formaldehyde (Merck) in 0.075 M phosphate buffer, pH 7.4 at room temperature, overnight. The tissue was removed from the fixative, rinsed thrice, 10 min each, in 0.075 M phosphate buffer. Tissue was then post-fixed in a 0.5% aqueous solution of osmium tetroxide (OsO_4) (SPI Supplies, West Chester, PA) for one hour. Thereafter, osmium tetroxide was removed and tissue was rinsed thrice, 10 min each, in 0.075 M phosphate buffer. Tissue was then serially dehydrated in 30%, 50%, 70% and 90% ethanol, followed by three changes of absolute ethanol for 15 min per dehydration step. For TEM analyses, tissue was then infiltrated with 30% Quetol (SPI Supplies, West Chester, PA) in ethanol for one hour, thereafter it was infiltrated with a 50% Quetol in ethanol solution for one hour. Finally tissue was infiltrated in 100% Quetol for a minimum of four hours. Immediately after infiltration, tissue was embedded in 100% Quetol epoxy resin (Van der Merwe and Coetzee, 1992) and polymerized for 39 hours at 60°C. Ultra thin serial sections (at an estimated thickness of 90nm each) were cut with a Reichert-Jung Ultra Cut E ultramicrotome (Vienna, Austria), and collected on copper grids. Tissue sections were contrasted for 10 min in 4% aqueous uranyl acetate in the dark and rinsed thrice in distilled water before it was contrasted for 5 min in Reynolds' lead citrate (Reynolds, 1963), thereafter it was rinsed again, three times in water. Samples were analysed with a JEOL JEM-2100F transmission electron microscope. All measurements were made with the aid of the Olympus iTEM analySIS software imaging system. Diameter was given as minimal Feret's diameter for any measured structure.

Muscle tissue samples from quadriceps belly area for SEM studies were dissected and fixed in the same way as for TEM analyses above. After the third dehydration step in absolute ethanol, samples

were stored in absolute ethanol until it was dried by critical point drying with liquid CO_2. Thereafter, samples were mounted and vaporized with ruthenium tetroxide (RuO_4) for one hour. Samples were analysed using a ZEISS ULTRA plus FEG SEM at 1kV.

Freeze-substitution

Small samples (0.2 x 1.2mm) were dissected from fresh tissue and mounted in hexadecene in a planchette. This was high pressure frozen using a Leica EM Pact II high pressure freezer. The samples were freeze substituted with acetone containing 1% OsO_4 using a Leica AFS2 freeze substitution unit. After substitution the samples were infiltrated and embedded with epoxy resin as for the chemically fixed material.

6.3 Results and Discussion

6.3.1 Ultrastructural Observations with TEM

The ultrastructure of quadriceps muscle from all the groups in the present study was assessed for specific and non-specific alterations. General morphology is shown in Figures 6.2 to 6.9, below. Different magnifications, as indicated by the scale bars, were utilized to visualize the structures of interest. SEM is a method for high-resolution imaging of surfaces that allow for very high magnification and greater depth of field (Denk and Horstman, 2004). Electron micrographs obtained with SEM analysis, provided insight on the surface structure of samples. Electron micrographs obtained by SEM analysis are presented in Figures 6.10 to 6.13, below.

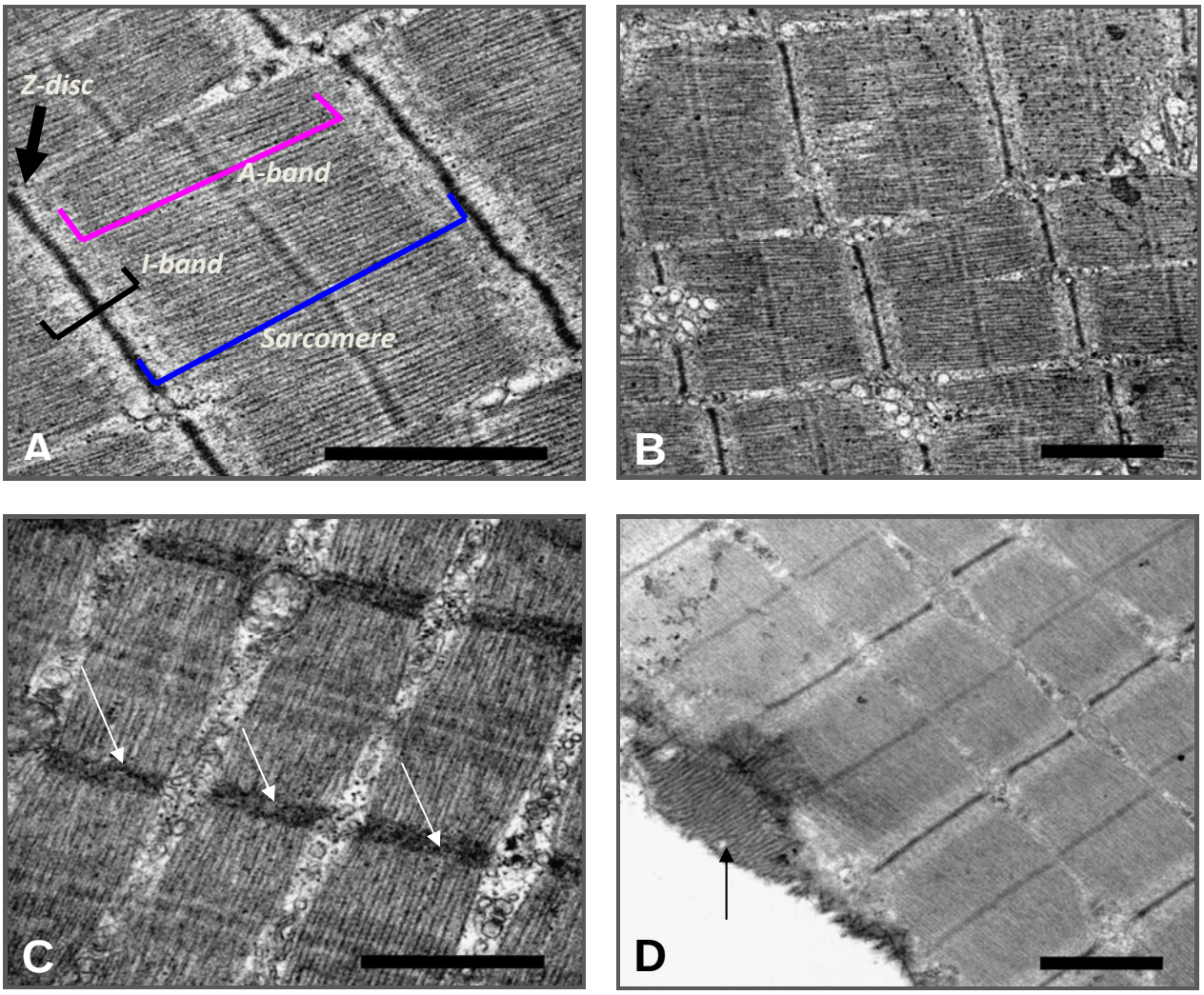

Figure 6.2: Electron micrographs from the negative control, SWR/J mice at 27 weeks of age that received placebo. A) Sarcomere and associated components. B) Small vacuoles between normal myofibers. C) Z-discs appeared thicker (arrows). D) Normal sarcomeres, with collagen fibers close to the periphery of the muscle fiber (arrow). Scale bars = 1µm

Negative control group

No structural abnormalities were observed in the 27 week-old SWR/J mice. Electron micrographs from this group (Figure 6.2) showed normal sarcomeres (A). Small bundles of vacuoles were seen in the Z-disk region. Generation of membranous structures are in response to normal membrane repair (Engel and Franzini-Armstrong, 2004). Mitochondria in this group displayed normal distribution between myofibrils at the level of the Z-disc, and in the subsarcolemmal position (B). Inner and outer mitochondrial membranes were found to be intact. Myofibrils in (C) displayed Z-discs that appeared slightly thicker than normal with no I-bands visible. It is expected that the muscle sample was possibly in contracting state upon fixation. Normal myofibrils (D) revealed normal sarcomeres with normal distribution of Z-discs, I-bands and A-bands. A small collagen bundle was observed on the periphery of the fiber in micrograph (D).

Figure 6.2 showed the distinct muscle tissue banding pattern corresponding to criteria for normal morphology. The Z-discs, A-bands, and I-bands are running at right angles to the long axis of the myofibrils. Sarcomeres were present in well defined units, and myofibrils aligned in an orderly manner. No abnormal distribution or dilatation was observed in the sarcoplasmic reticulum or the T-tubule systems. The plasma membranes appeared to be intact, with no vesicles observed in the subsarcolemmal position.

Age control group

Relatively large mitochondria were present in the subsarcolemmal position (A) of samples from the age control group, SJL/J mice at 14 weeks of age that received no treatment (Figure 6.3). Cristae were visible inside mitochondria, in addition to small spaces that appeared optically empty. This observation may be due to degenerative changes. In the same micrograph (A) small vacuoles, similar to that seen in the negative control group were seen. Vesicles accumulating under the sarcolemma were observed.

Any abnormal space or cavity in a muscle fiber may be considered a vacuole (Carpenter and Karpati, 1984). In Figure 6.3 (B), vacuoles that appeared optically empty were present. These vacuoles showed an irregular periphery, and they could be expected to be derived from mitochondrial vacuolation. Between these vacuoles, mitochondria with similar shapes as the vacuoles were observed. A tubular structure (B, arrow) was observed in the same area. Inside these mitochondria, dense cristae were visible (C). Cristae showed normal distribution, in relatively large mitochondria found in the intermyofibrillar position. Vacuole formation was observed in some mitochondria (D).

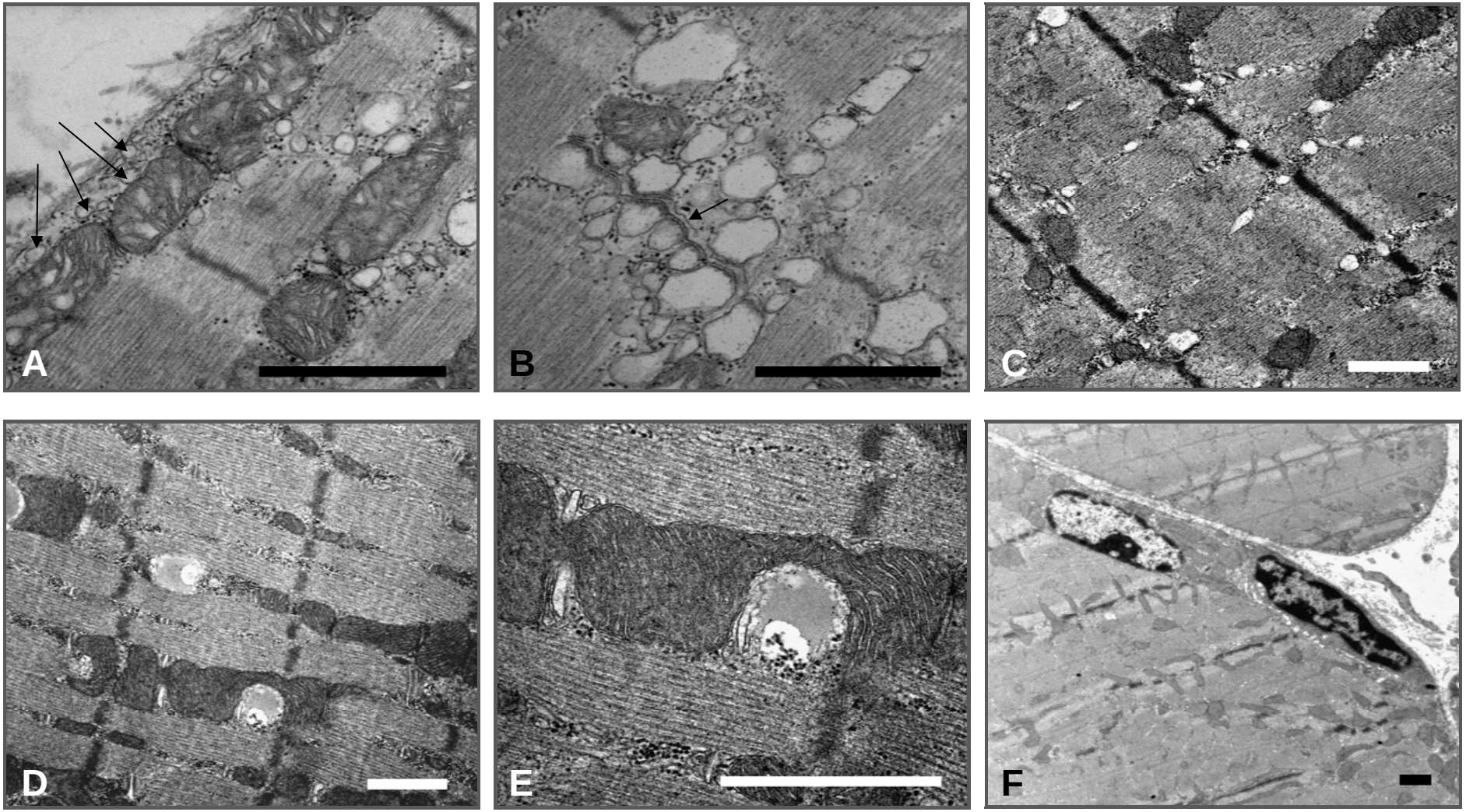

Figure 6.3: Electron micrographs from the age control group, SJL/J mice at 14 weeks of age that received no treatment. A) Mitochondria in the subsarcolemmal position and between myofibrils. The arrows point to vesicles accumulating under the sarcolemma. B) Empty vacuoles in a Z-disc position. The arrow point to a tubular structure in the region. C) Prominent Z-discs in healthy appearing myofibrils, intercepted by the presence of small vacuoles. D & E) Vacuoles between mitochondria. F) A myonucleus (left) and satellite cell (right). Scale bars = 1µm

At higher magnification (E) the vacuole in (D) appeared to have formed as a result of degeneration of a mitochondrion. On closer investigation it was established that the boundary of the vacuole was a double membrane structure, that of the mitochondrion. It was therefore evident that the mitochondrion was positioned around the vacuole and not invaded by it. In addition, no degenerative changes to the inner or outer membranes were visible in this mitochondrion either. The vacuole contained membranous structures, a lipid droplet, and glycogen particles. The cristae of the affected mitochondria were not dilated and showed normal distribution.

A satellite cell (F, right) was observed in the space between the plasmalemma and the basal lamina. These small, flattened cells are found in close proximity to the myofibril with an intervening space of ≈15nm between the plasmalemma and the satellite cell (Ovalle *et al*., 2008). This position enables the observer to differentiate between satellite cells and myonuclei (F, left). Satellite cells are the muscle's own population of stem cells and have the ability to repair or regenerate damaged segments of muscle fibers.

Positive control group

Figure 6.4 represents a series of electron micrographs from the positive control group, SJL/J mice at 27 weeks of age that received placebo. Myofibrils are bundles of thick and thin myofilaments in orderly arrangement with periodic Z-discs (Carpenter and Karpati, 1984). An interruption of this orderly arrangement was observed (A). Myofibrillar arrangement was intermittent with areas of myofibril loss (asterisk), suggestive of necrotic changes. Considering the low magnification of this micrograph, it is unlikely that the myofibrils simply left the plane of sectioning. It is more likely that they are affected by degeneration, as parts of the affected areas appear empty.

A longitudinal section through a muscle fiber (B) from this group displayed the tendency of thin filaments to bend (double bracket) in a muscle which is fixed in a relatively contracted state, in view of the length of the I-band. This bend that occurred in the middle of a myofibril caused the myofibril to split. From micrograph (B), it is evident that the split was initiated by an alteration to the tubular system, presumably dilatation of the sarcoplasmic reticulum or T tubules.

Myofibrils from this group showed smallness and in some instances the myofibrils were contracted, resulting in the appearance of a thickened Z-disc (C). It is possible that this muscle sample was in a contracting state upon fixation. Degenerative changes were observed in this group between myofibrils (D), characterized by large open spaces, dilated tubules, and mitochondrial remnants.

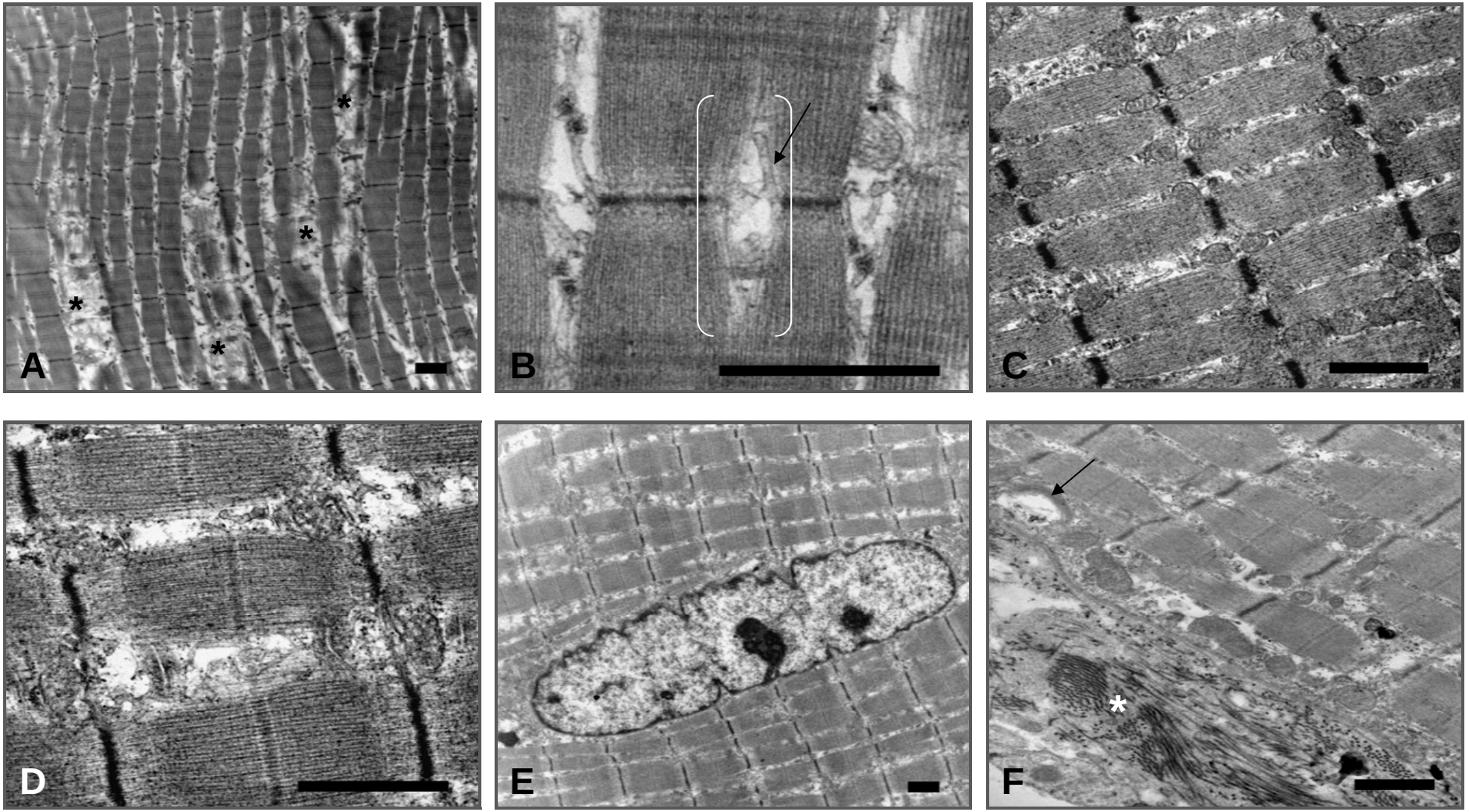

Figure 6.4: Electron micrographs from the positive control group, SJL/J mice at 27 weeks of age that received placebo. (A) Myofibrillar disruption that leads to myofibrillar loss due to necrosis (asterisks). (B) A bent in the myofibril at the level of thin filaments (double bracket) with dilated tubules (arrow) visible. (C) Small myofibrils in a state of hypercontraction. (D) Degenerative changes characterized by large open spaces, dilated tubules and mitochondrial remnants between myofibrils. (E) A myonucleus in the central position of a fiber. (F) Subsarcolemmal vacuoles (black arrow) are present. Collagen fibers (asterisk) can be seen in the extracellular spaces. Scale bars = 1µm

Light microscopy (in chapter 5) revealed that myonuclei situated in the central position of myofibers were quite common in this group, with the highest prevalence, compared to all other groups. Cytoplasmic invaginations were observed to the nucleus in Figure 6.4 (E) that is situated in a central position of the fiber. This incidence points to the difference seen between nuclei in this group, compared to nuclei from the age control group (Figure 6.3, F), which lack invaginations into nuclei, but is consistent with nuclei found in the negative control samples (data not shown). The mechanism behind this structural alteration is not known. Subsarcolemmal vacuoles (F, black arrow) were present in samples from this group. Collagen fibers (F, asterisk) were present in the extracellular spaces.

Resveratrol group

Electron micrographs taken from muscle samples of animals treated with resveratrol (Figure 6.5), revealed myofibrils that showed more consistency in size and less disruption of whole myofibrils (A) compared to the positive control group. Mitochondria detected in samples that were freeze-substituted displayed a relative normal distribution (B). Higher magnification (C) showed larger numbers of mitochondria in subsarcolemmal regions. These mitochondria displayed a variation in shapes ranging from oval to round. Cristae were not clearly visible in freeze-substituted samples.

Micrograph (C) showed a sarcolemmal gap (*) measuring 0.63µm, as well as thickening of the basal lamina measuring up to 0.5µm. Glycogen particles were visible in the sarcoplasm. Vacuolation was observed (B and D) that differs from that seen in the age control and negative control groups. They were slightly bigger, mostly empty, and were found scattered between myofibrils in conjunction with mitochondria. Myofibrils in this group revealed a more orderly arrangement of thick and thin filaments.

Micrograph (E) revealed that mitochondria in this group were severely challenged, and that the vacuoles observed in (D) could possibly be derived from mitochondrial degeneration. The centres of these vacuoles appeared optically empty and bounded by a membranous structure. The affected mitochondrion (E and F) displayed large open optically empty spaces, indicative of degenerative changes. Some of the vacuoles were empty while others showed remnants of what used to be the cristae (E). There were membranous whorls with a few glycogen particles present in the centre of the degenerating mitochondrion (F).

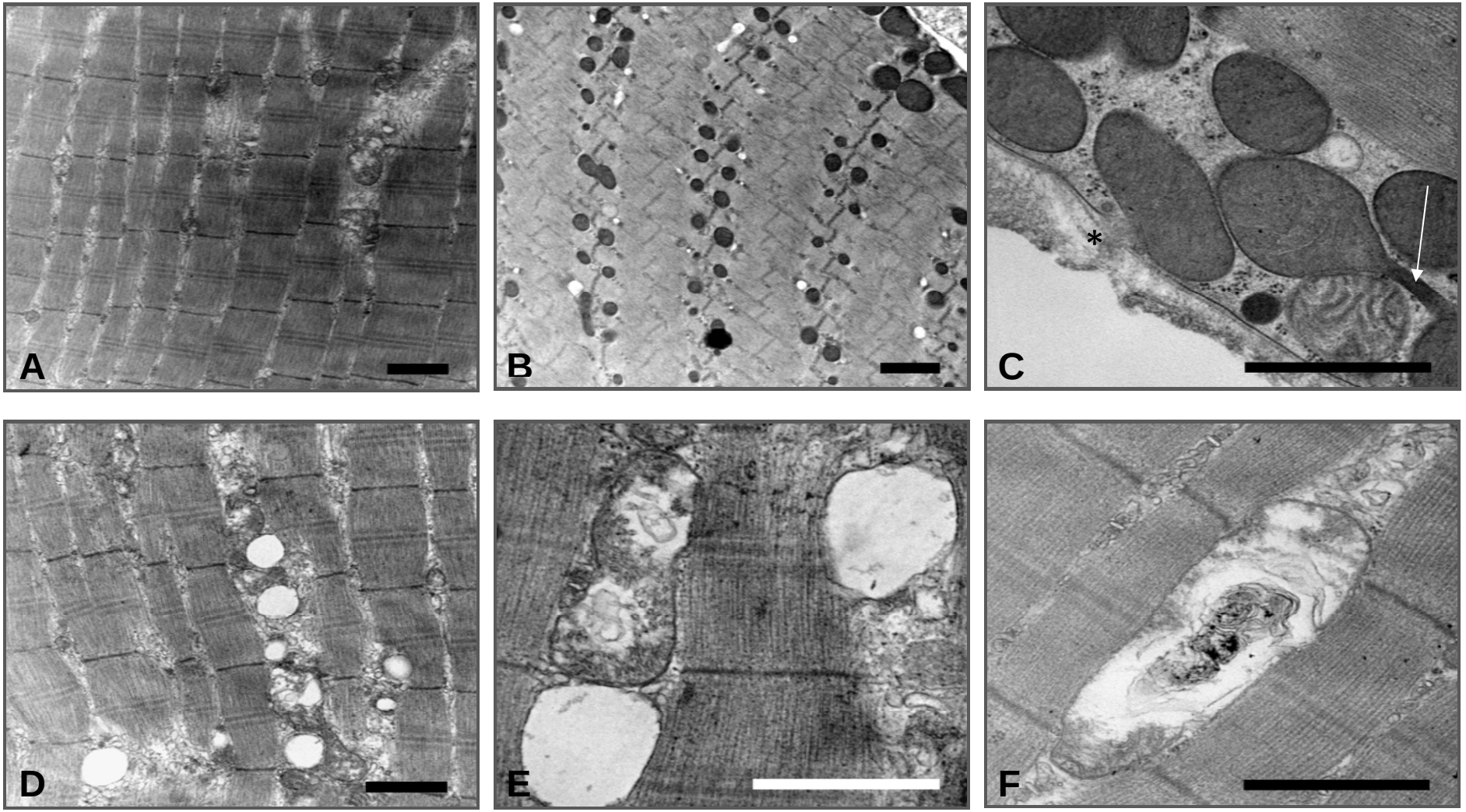

Figure 6.5: Electron micrographs from the resveratrol group. (A) Occasional myofibrillar degeneration. (B) Mitochondria show normal distribution, with large numbers found in the subsarcolemmal position (C). A plasmalemmal gap and basal lamina thickening is present on this freeze-substituted sample (C). A disruption in the plasma membrane is present (*)A strange connection (C, arrow) of unknown origin between two mitochondria. Vacuoles (D) can be observed between myofibrils, presumably resultant from mitochondrial degeneration. (E & F) Degeneration of a mitochondrion. Scale bars = 1µm

Low CoQ10 group

Figure 6.6 showed electron micrographs taken from samples representing the low CoQ10 group. Myofibrillar disruption (A and B) lead to unorderly arrangement of myofibrils in this group. Larger magnification (B) showed disruption of the Z-disc stability. In some instances the Z-disc disappeared (black arrow) in some myofibrils. Thick filament instability resulted in myofibrillar splitting (white arrow).

Micrograph (C) revealed that the thin filaments were also affected, resulting in splitting of part of a myofibril at the level of the I-band (black arrow). Plasmalemmal discontinuities, characteristic of dystrophic changes in muscle, were observed and included subsarcolemmal vesicles, membrane bound vesicles, and subsarcolemmal glycogen particle accumulation (C, white arrows).

Indentations into the membrane that was first observed by light microscopic analysis in this group and others, in chapter 5 (Figures 5.7.1, C and D), was now observed at the ultrastructural level (D and E). Ultrastructural analysis (D) revealed that these indentations might be the result of inflammatory infiltration by inflammatory cells and processes, and the pressure exerted on the fiber by these processes. Ultrastructure of this incident revealed an almost orderly spherical arrangement of myofibrils around the affected area (E).

In order to afford this arrangement of myofibrils, there has to exist a certain degree of structural adjustment in the myofiber. Micrograph (E) showed that this suggestion could hold truth, as there is a severe disruption of the normal myofibrillar structure, including Z-disc loss, and thick and thin filament disruption. Carpenter and Karpati, 1984, reported that Z-disc loss may occur in the early events of necrosis, and that this loss might be caused by activation of enzymes like proteases. It is also possible, due to the orientation of the fibrils around the indentation, that they simply leave the plane of sectioning, and appear disrupted. Investigation of the surface morphology by SEM will bring this finding to a close (Section 6.4; Figure 6.13).

Collagen bundles (F, asterisk) were also detected around fibers in this group.

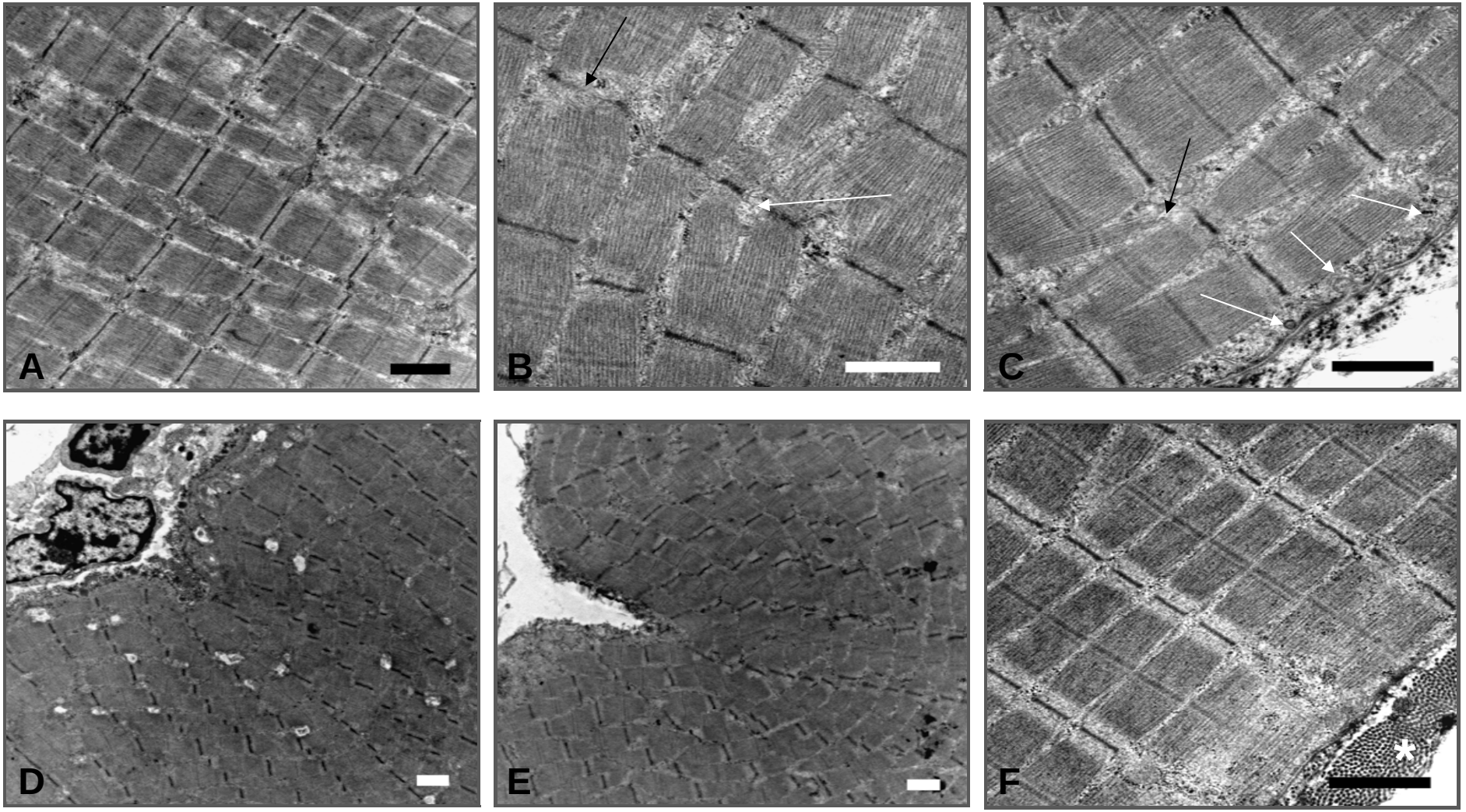

Figure 6.6: Electron micrographs from the low CoQ10 group. (A & B) Myofibrillar disruption leads to unorderly arrangement of myofibrils in this group. Larger magnification (B) shows Z-disc loss (black arrow) in some myofibrils as well as thick filament disorientation that resulted from myofibrillar splitting (whit arrow). (D) Myofibrillar arrangement around indentations in myofibers. Inflammatory cells, presumably macrophages, are present at the indent. (E) Thick and thin filament disorientation and probable Z-disc loss in myofibrils arranged around a fiber indent. (F) Collagen bundles (asterisk) were present around fibers in this group. Scale bars = 1µm

High CoQ10 group

Qualitative ultrastructural analysis of quadriceps muscle samples from the group treated with a high dose of CoQ10 (Figure 6.7) revealed intact membranes (A, black arrow) and overall less occurrence of membrane discontinuities, on a transverse section (A). The sarcoplasmic reticulum was observed in the perimyofibrillar position with no dilatation observed in the present micrograph. On the contrary, the basal lamina appeared thickened (A, white arrow) and presumably represents duplication. This is a known characteristic of dysferlin-deficient muscle membranes, observed by Selcen and co-workers (2001) and Cenacchi and co-workers (2005).

Freeze-substituted samples (B) showed membrane discontinuities, including small gaps, ranging from 0.08 to 0.2µm, and vesicles in the subsarcolemmal position. This electron micrograph also showed multiple, small globules of dense material embedded in a thickened basal lamina.

Numerous vacuoles were present in some regions, usually surrounding mitochondria (C) and between myofibrils (D). The mitochondrion in micrograph (C) appeared normal. The vacuoles in micrograph (C) were not optically empty; tiny particles were scattered throughout the visible centers. Mitochondria were found between myofibrils (C and D) and under the sarcolemma. Cristae were observed in most instances, although some mitochondria displayed tiny areas that appeared optically empty (D, white arrows).

Z-disc streaming, a common lesion, seen in numerous conditions and situations, was observed in one sample from this group (D, white arrow). Carpenter, 2001 (b) explained that it combines a mild focal loss of myofilaments and loss of the Z-disc lattice with streaming of the material of the Z-disc along either thin or remaining thick filaments. Micrograph (D) clearly showed that the streaming extends from one Z-disc to the neighbouring Z-disc, with the parts of Z-discs on the periphery of the myofibril, spared. The target fibers in denervating conditions, has shown that this phenomenon manifests in areas lacking mitochondria, but may actually be a manifestation of reinnervation (Carpenter, 2001 b). Since mitochondria were observed in the surroundings of the myofibril affected by Z-disc streaming, this finding might be suggestive of reinnervation. Numerous small spherical structures, presumably vacuoles, were visible around the affected myofibril. The myofilaments of the affected myofibril appeared optically transparent, compared to the other myofibrils.

Bending of myofibrils around an indentation (E) was observed in the present group.

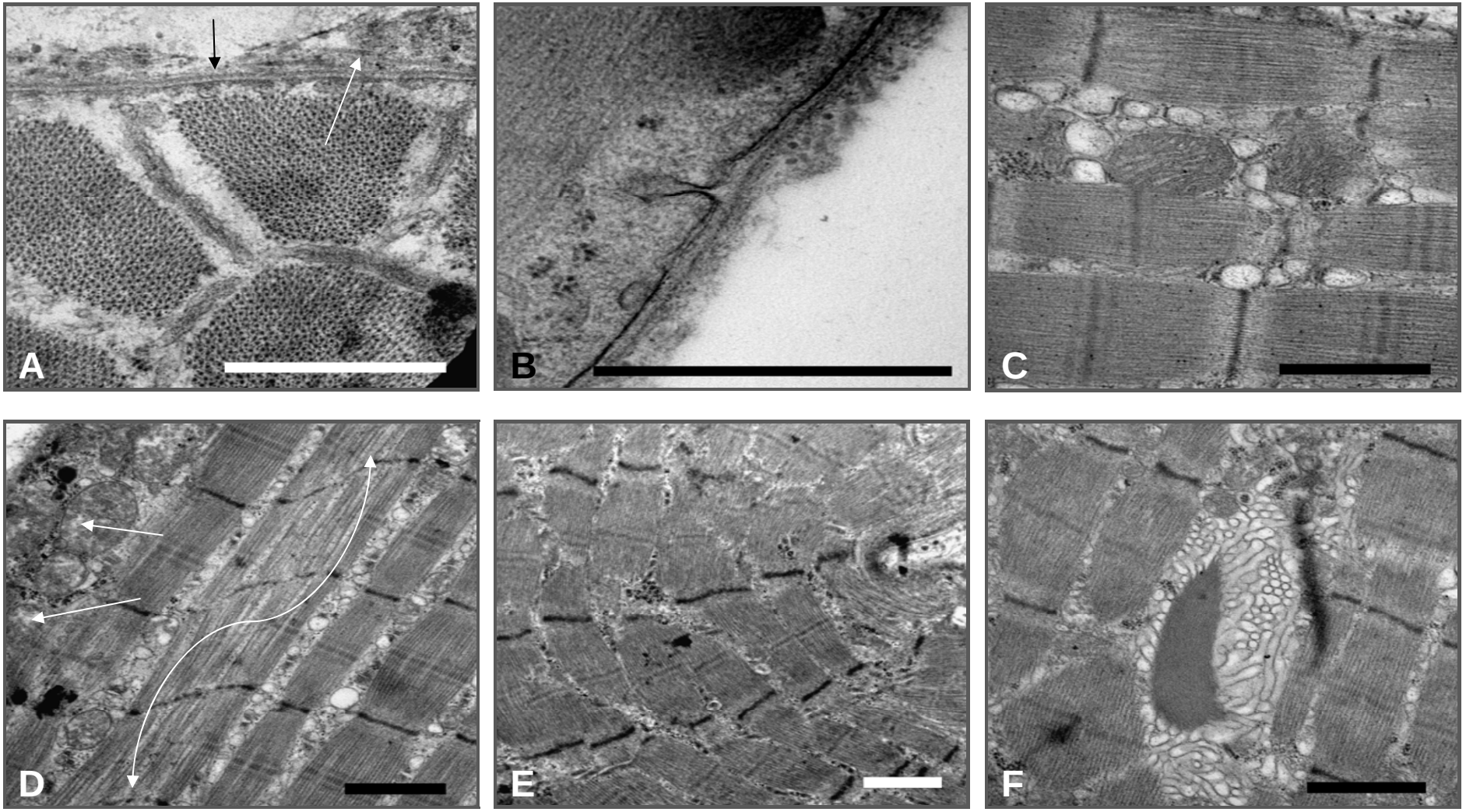

Figure 6.7: Electron micrographs from the high CoQ10 group. (A) An intact membrane (black arrow) on a transverse electron micrograph with a thickened basal lamina (white arrow). (B) Plasmalemmal discontinuities are present in some areas. (C) Small vacuoles can be seen between myofibrils. (D) A fiber in which Z-disc streaming (arrow) occurred. Some mitochondrial displayed areas that appeared optically empty (white areas). (E) Myofibrils bend around an indentation in a myofiber. (F) An area of focal accumulation of tubular structures surrounding a myofibril-like segment. Scale bars = 1µm

Another strange occurrence observed in this group was a focal dense area of tubular structures aggregated around a myofibrillar-like segment (F). The well defined tubular structures (F) were found to surround a part of what appeared morphologically similar to a myofibril that lacks any characteristic banding, but showed a similar surface structure to thick filaments. The structure was found between other myofilaments and the tubular structures that surrounded it. The tubular structures were found to be orientated in longitudinal and transverse positions and are supposedly derived from either one or all of the following; the T-tubule-, golgi-, and/or sarcoplasmic reticulum systems. This phenomenon was not observed in any of the other groups in the present study.

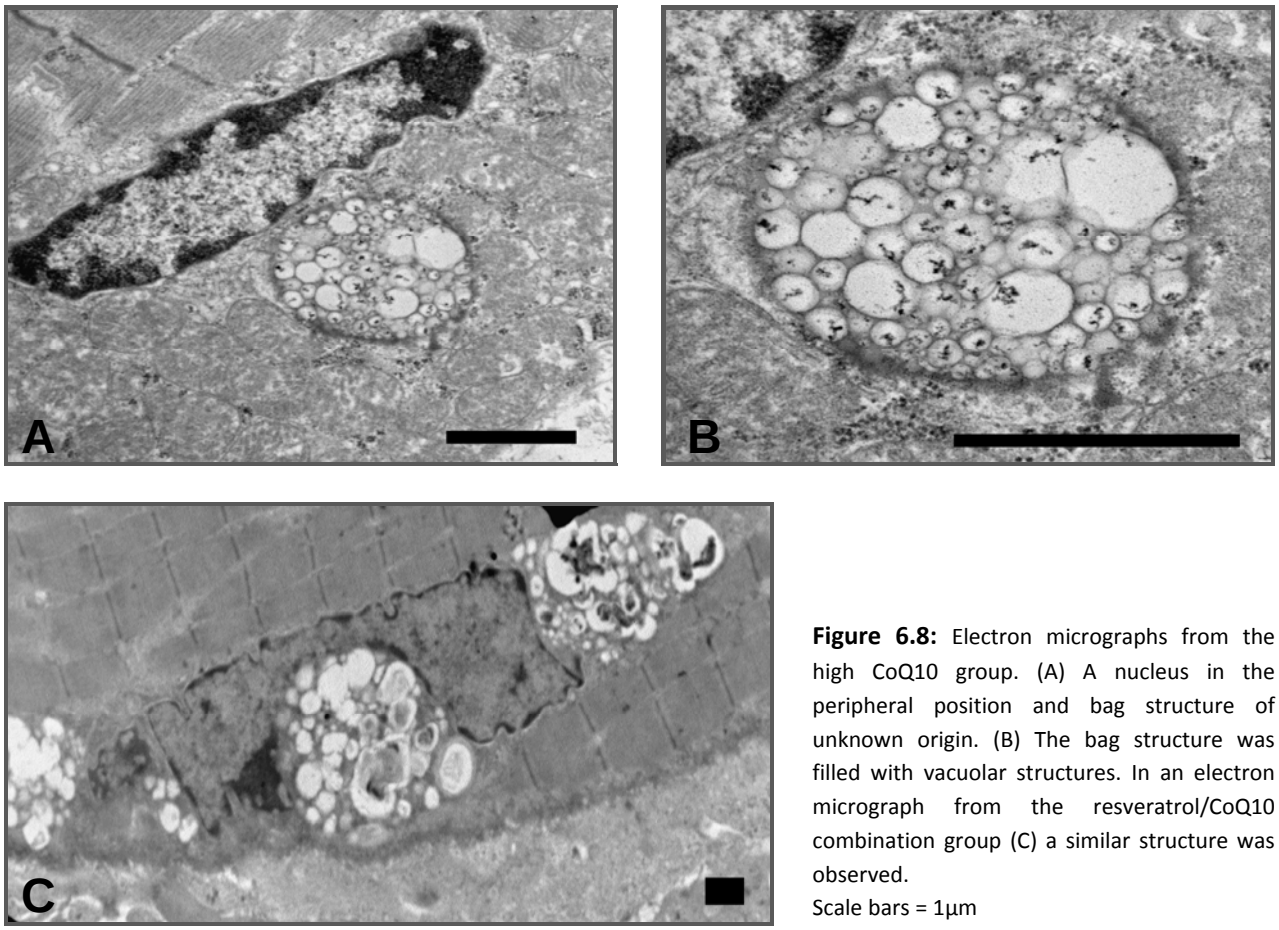

Figure 6.8: Electron micrographs from the high CoQ10 group. (A) A nucleus in the peripheral position and bag structure of unknown origin. (B) The bag structure was filled with vacuolar structures. In an electron micrograph from the resveratrol/CoQ10 combination group (C) a similar structure was observed.
Scale bars = 1µm

A nucleus (Figure 6.8, A) located near the periphery of a fiber from the same group, was found to be surrounded by a very large number of mitochondria (A), which is not uncommon. A strange bag structure bound by an optically dense structure (A and B), and filled with small membrane bound vacuolar organelles, was observed in close proximity to the nucleus. The structure was of unknown origin. A similar occurrence was observed near a peripherally located nucleus in the resveratrol/CoQ10 combination group (C). The structure was invading a degenerating nucleus and lacked a clearly defined boundary.

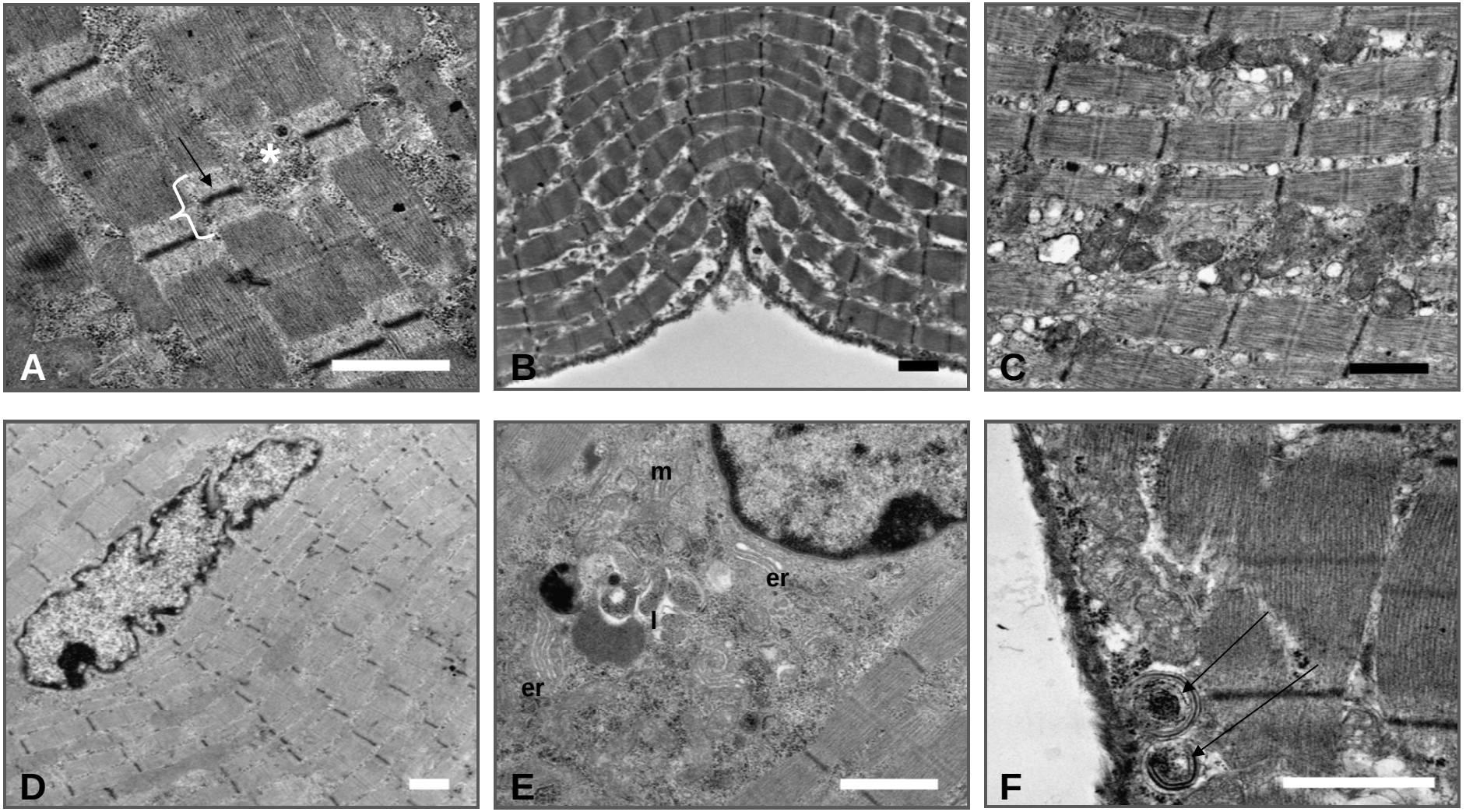

Figure 6.9: Electron micrographs from the resveratrol/CoQ10 combination group. (A) Myofibrils show 'missing' I-bands (asterisk), this does not represent myofibrillar loss or breakdown, and is just an effect of sectioning. The I-bands appear distinctly long in size (white brace). (B) Myofibrils bend around an indentation in a myofiber. (C) Mitochondrial and vacuole accumulation in areas of myofibrillar disruption. (D) A centrally located myonucleus. (E) The area around a central nucleus. Endoplasmic reticulum (er), mitochondria (m), round spaces, presumably lysosomal (l) which contained dense debris and glycogen particles are visible. (F) Membranous whorls (arrows) beneath the sarcolemma. Scale bars = 1µm

Resveratrol/CoQ10 combination group

Electron micrographs from the resveratrol/CoQ10 combination group are represented by Figure 6.9. Micrograph (A) revealed myofibrils that showed 'missing' I-bands from the myofibrils, that otherwise appeared to be in good condition (A, asterisk). These regions were focally dense with glycogen particle accumulation. Glycogen particles were also found between myofibrils.

Carpenter, 2001 (b), reported that they have seen selective I-band loss only rarely, focally in a few fibers, and only in denervating conditions. I-band loss has been demonstrated by Carpenter and Karpati, 1984, where it was shown that when the I-bands in myofibrils are lost, it result in blocks of thick filaments that became disorientated, and the orderly appearance seen in micrograph (A) is unavoidably lost. Carpenter and Karpati, 1984, reported that far too many micrographs of longitudinal sections have been interpreted as showing myofibrillar loss, or lysis, where the myofibrils simply leave the plane of sectioning. The myofibrils seen in (A) were in good order, yet the I-bands appeared missing. This observation has been shown by Carpenter and Karpati, 1984, to be purely an effect of sectioning. Therefore, the finding in (A) did not correspond to myofibrillar loss or breakdown.

Myofibrils in samples from this group were also found to bend around indentations in myofibers (B). Myofibrils were subjected to disruption, and mitochondria and vacuoles, accumulated at affected areas(C). Vacuoles were small but numerous.

A myonucleus found in the central position between myofibrils (D) showed deep invaginations, where it almost lead to a split in the nucleus. Nuclei that were divided into two separate parts were also observed in the present group. These nuclei were always found in a central position. The area around a central nucleus (E) displayed numerous mitochondria (m), endoplasmic reticulum (er), and round spaces, presumably lysosomal (l) which contained dense debris and glycogen particles.

Membranous whorls (F) were observed in one sample from this group. These two structures in micrograph (F) measured 0.41 and 0.54µm respectively, and are also known as myelin figures and/or myeloid bodies. Membranous whorls are often associated with a vesicular space whose walls they line (Carpenter and Karpati, 1984). Electron microscopy studies by Carpenter and Karpati, 1984, revealed that they are formed from cytomembranes, in a circumferential arrangement with a variable periodicity. Similar to the membranous whorls in inclusion body myositis (Carpenter and Karpati, 1984), the centers of the whorls found in the present study in SJL/J mice, were also occupied by glycogen particles.

6.3.2 Unravelling the Ultrastructural Findings

The main ultrastructural alterations in the sarcoplasmic compartment were found to be non-specific architectural changes. These include mild or severe loss of myofilaments (Figure 6.11), dilated sarcoplasmic reticulum and T system profiles, and degenerative changes of the mitochondria. In addition, large vacuoles containing myelin-like lamellae, and myofibrils orientated around indentations into the fiber, were observed. Central nuclei were often observed, in addition to many lipid vacuoles and mitochondrial aggregates, in both the intermyofibrillar and subsarcolemmal regions. These changes occur in all SJL/J animals. They were found to be more pronounced in the positive control group. Since ultrastructural analysis makes use of ultrathin resin sections (≈90nm), the field investigated is limited, and the findings are therefore discriminating within the same strain, between treated and untreated groups.

Specific alterations of muscle fibers from molecularly diagnosed dysferlinopathy samples were identified by Cenacchi and co-workers, 2005. They found that the ultrastructure of the surface cell layer at the level of the sarcolemma and basal lamina showed few sarcolemmal gaps and many elongated microvilli-like projections. The basal lamina was also found to be thickened or multilayered, and seemed to include some globular aggregates of amorphous electron dense material.

Similar observations were made in the present study, where the basal lamina measured up to 0.5µm (Figure 6.5, C). On investigation of the subsarcolemmal region it was found to be characterized by the presence of several aggregates of small vesicles, which presumably derived from the golgi apparatus. Most membrane defects were found to be small gaps, ranging from 0.08 to 0.63µm. Extensive plasmalemmal defects were typically found in necrotic fibers that were denuded of most of their surface membrane. These extensive membrane discontinuities were mostly detected in the positive control group of the present study. Plasma membrane defects were also present on non-necrotic fibers in all groups of SJL/J mice. In addition sarcolemmal replacement by one to multiple layers of small vesicles, were observed in most groups.

The investigations of the present study also paid attention to non-specific alterations on ultrastructural level; a sparsely described subject in the literature on dysferlinopathies. These changes included vacuolation, unorderly myofibrillar arrangement, and mitochondrial localization and structure.

Vacuoles

Vacuoles in skeletal muscle can be of many sorts (Carpenter, 2001 a). The contents of a vacuole may be stainable or appear optically empty, because the contents have dissolved or diffused out in processing (Carpenter and Karpati, 1984).Material such as glycogen can be carried artefactitiously into otherwise clear vacuoles (Carpenter, 2001 a). A vacuole can arise from various pre-existing organelles.

Small subsarcolemmal and intermyofibrillar vacuoles were detected in all groups analysed, including the SWR/J mice that served the negative control. Vacuoles described by Selcen and coworkers, 2001, were found either close to or abutted on the sarcolemma. The present study revealed numerous vacuoles in the subsarcolemmal position, but also in the intermyofibrillar position, often at the level of the I-band, and often associated with the presence of mitochondria nearby. They appeared singly or in clusters, and were either empty or contained degraded membrane fragments. Occasionally small, optically dense material was observed in their centers. Some vacuoles were found abutted on membranous networks of the T tubule system and/or sarcoplasmic reticulum.

The T-tubule system serve as membrane source for membrane bound vacuoles and vesicles in muscle (Klinge *et al*., 2007) and is involved in the generation of membrane for elongation and repair purposes of the sarcolemma, and to 'react' in regenerating muscle fibers (Engel and Franzini-Armstrong, 2004). Selcen and co-workers, 2001, have shown that subsarcolemmal vacuoles contiguous with the T-tubule system are one of the ultrastructural hallmarks of dysferlinopathy muscle. Klinge and co-workers, 2007, have shown that dysferlin accumulation at wounding sites in early myogenesis, are derived from a T-tubule localization. The T-tubule system appears to serve as a pool of dysferlin positive endomembrane in the process of membrane repair (Klinge *et al*., 2007). It is therefore possible that in areas of larger membrane disruptions where the fiber is challenged by large sarcolemmal degeneration, more vacuoles and vesicles will be present in the affected fiber, to provide a membrane source for repair (Figure 6.3, A and B).

As vacuoles have been detected in many muscle pathologies, it created the idea that vacuolation occurs in response to necrosis. Taking into consideration the work of others (Selcen *et al*., 2001; Klinge *et al*., 2007), it became apparent that vacuolation occurred in response to membrane damage as a first line attempt to repair the membrane injury. The present study found vacuoles in SJL/J quadriceps muscle of all groups, treated and untreated. The largest vacuoles, in the present study, as a result of mitochondrial vacuolation, were found in the resveratrol group (Figure 6.5 E and F).

Numerous smaller vacuoles and vesicles were detected in groups treated with a high dose of CoQ10 and resveratrol/CoQ10 in combination.

Mitochondria

The β-oxidation of fatty acids, the Krebs cycle, the respiratory chain and ATP synthase are located in the mitochondria, where a large proportion of the energy used by muscle cells is made available (Carpenter, 2001 b). In muscle cells, mitochondria are usually concentrated in four locations, between myofibrils at the I-band level, under the sarcolemma, at the motor endplate and at the poles of myonuclei (Carpenter, 2001 b).

The functional activity of the mitochondria greatly influences the extent of reactive oxygen species (ROS) formation. Low levels of ADP and high mitochondrial membrane potential give high levels of ROS. In turn high ADP levels and low membrane potential result in low levels of ROS production (Bentinger *et al*., 2007).

In the present study, numerous mitochondria of different shapes and sizes were observed in all groups under investigation. Some mitochondria in the age control group (14 week old SJL/J mice), displayed small empty spaces between cristae (Figure 6.3, A), while others showed dense distribution of cristae and were found to be larger in size (Figure 6.3, D). Mitochondria in the intermyofibrillar position of the positive control group, were found to be smaller in size (Figure 6.4, C), and in some samples appeared to undergo degenerative changes (Figure 6.4, D and F).

Large mitochondria were observed in the group supplemented with resveratrol. Some mitochondria in this group showed a normal distribution pattern under the sarcolemma and between myofibrils (Figure 6.5, B). In other samples from the same group mitochondria had undergone degenerative changes (Figure 6.5, A and D), leading to the formation of large vacuoles (Figure 6.5, E and F). Mitochondria were present in both CoQ10 groups and the resveratrol/CoQ10 combination groups, with little to no pronounced alterations observed.

Studying the morphology of mitochondria on an ultrastructural level, gives a good indication of the size, distribution and shape of the mitochondria. It is nevertheless difficult to make any conclusions on how dysferlin-deficiency exactly affects the mitochondria. It is also not possible to derive an exact conclusion on the effect of antioxidant supplementation on the mitochondria, as their alteration by the disease itself is not yet fully understood. It can be expected that, if the supplementation of antioxidants does affect the mitochondria *per se*, it will need to be confirmed by molecular analysis.

An apparent random distribution of alterations in mitochondria included swelling, considerable variation in size, and disintegration of the characteristic shape of the cristae, with general disorganisation of the inner membrane being evident usually in swollen mitochondria. The outer membrane appeared to be intact, almost in all instances. In some mitochondria from the positive control, low CoQ10 and resveratrol groups, the inner membrane was completely disrupted, resulting in the formation of intramitochondrial vacuoles. In some instances, open spaces occurred in regions, presumably once occupied by mitochondria. Smaller mitochondria were observed in the high CoQ10 and resveratrol/CoQ10 groups. These findings imply that the ongoing dystrophic changes in the SJL/J mouse are affecting the mitochondria, and that the alterations are less pronounced in the high CoQ10 and resveratrol/CoQ10 groups.

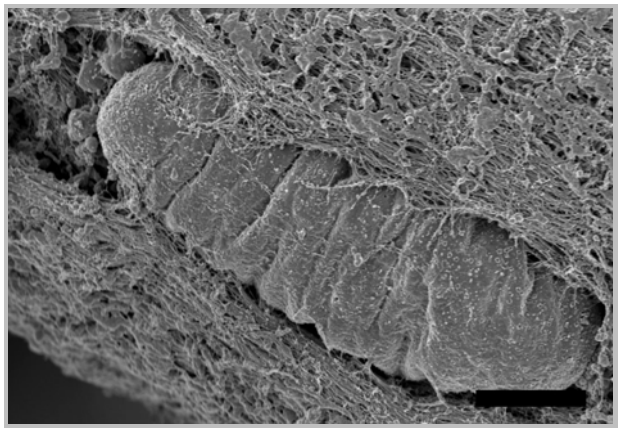

Figure 6.10: A scanning electron micrograph of a mitochondrion in the subsarcolemmal position from the age control group. The mitochondrion appears normal, but the sarcolemma is disrupted.
Scale bar = 2µm

The mitochondrial ultrastructural changes observed in SJL/J mice are consistent with the findings of Haycock and co-workers, 1996. Their team showed that mitochondrial ultrastructural alterations, similar to what was found in the present chapter, were the result of ROS-induced oxidative damage. A novel experimental approach by Haycock's group was employed to quantify the relative susceptibility of membrane-associated, contractile and mitochondrial proteins in normal human muscle tissue sections, to oxidative damage by ROS. The authors found that different proteins, differing in structure, function or intracellular localization, showed different susceptibility to oxidative damage. They found certain mitochondrial proteins (succinate dehydrogenase, cytochrome oxidase) to show particular susceptibility. In addition, ultrastructural analysis of subcellular organelle damage, revealed particular susceptibility of mitochondria to ROS-induced oxidative damage (Haycock *et al*., 1996). Haycock and co-workers, 1996, reported the possibility that mitochondria can tolerate a critical maximum volume of ROS induction, thereafter oxidative stress insult will result in bursting of the outer membrane, leading to the formation of small vacuolar spaces.

The finding of numerous small vacuolar spaces is consistent with this theory, further strengthening the possibility that the disruption to mitochondria in SJL/J muscle are the result of oxidative stress insult. Of further interest, was the observation of severely altered mitochondria in the resveratrol group but not in other antioxidant supplemented groups. This observation might suggest that resveratrol alone cannot protect mitochondria from the critical maximum volume of ROS that can be tolerated, but the higher dose antioxidant supplementations, afforded protection against these mitochondrial alterations.

It is therefore possible that higher concentrations of antioxidants reduced the level of ROS in the cell, thereby reducing the maximum volume of ROS 'attacking' the mitochondria. This action will result in less damage to mitochondrial ultrastructure, as was seen in the high CoQ10 and resveratrol/CoQ10 combination groups. To support this theory, further investigation on the effect of antioxidant supplementation on lipid peroxidation levels in the present model was done and reported in chapter 7.

6.3.3 Ultrastructure on the Surface

SEM has previously been found to provide a powerful tool for qualitative ultrastructural analysis when focussing on the surface integrity of tissue (Potgieter *et al*., 2009). SEM was utilized to shed more light on the surface integrity of muscle tissue in the present study (Figures 6.10 to 6.13). Although electron micrographs obtained by this analysis greatly lacked information specific to the pathology, it provided interesting information on the surface structure of the tissues examined by TEM. Figure 6.11 revealed how myofibrillar arrangement is distorted in the 27 week-old untreated SJL/J mice, compared to that of the negative control SWR/J mice.

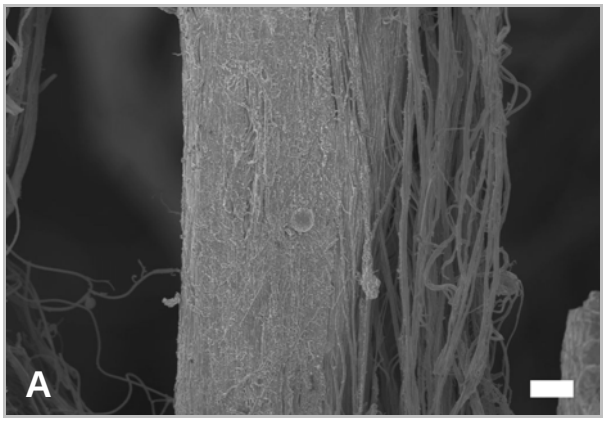

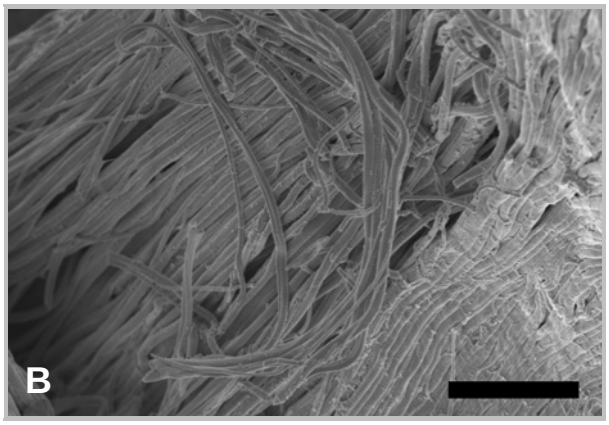

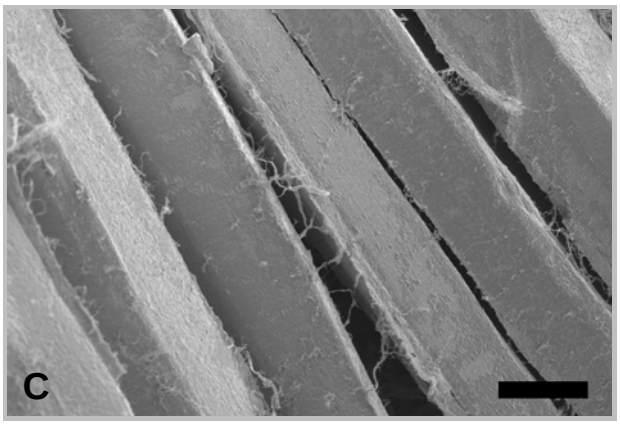

Figure 6.11: Scanning electron micrographs showing myofibrillar disruption and loss in the placebo treated positive control group (A & B), and solid fibers (C) from the negative control group. Scale bar = 2µm

Figure 6.12 displayed electron micrographs taken on the surface of muscle fibers, revealing the shape and size of vesicles accumulating under the membrane.

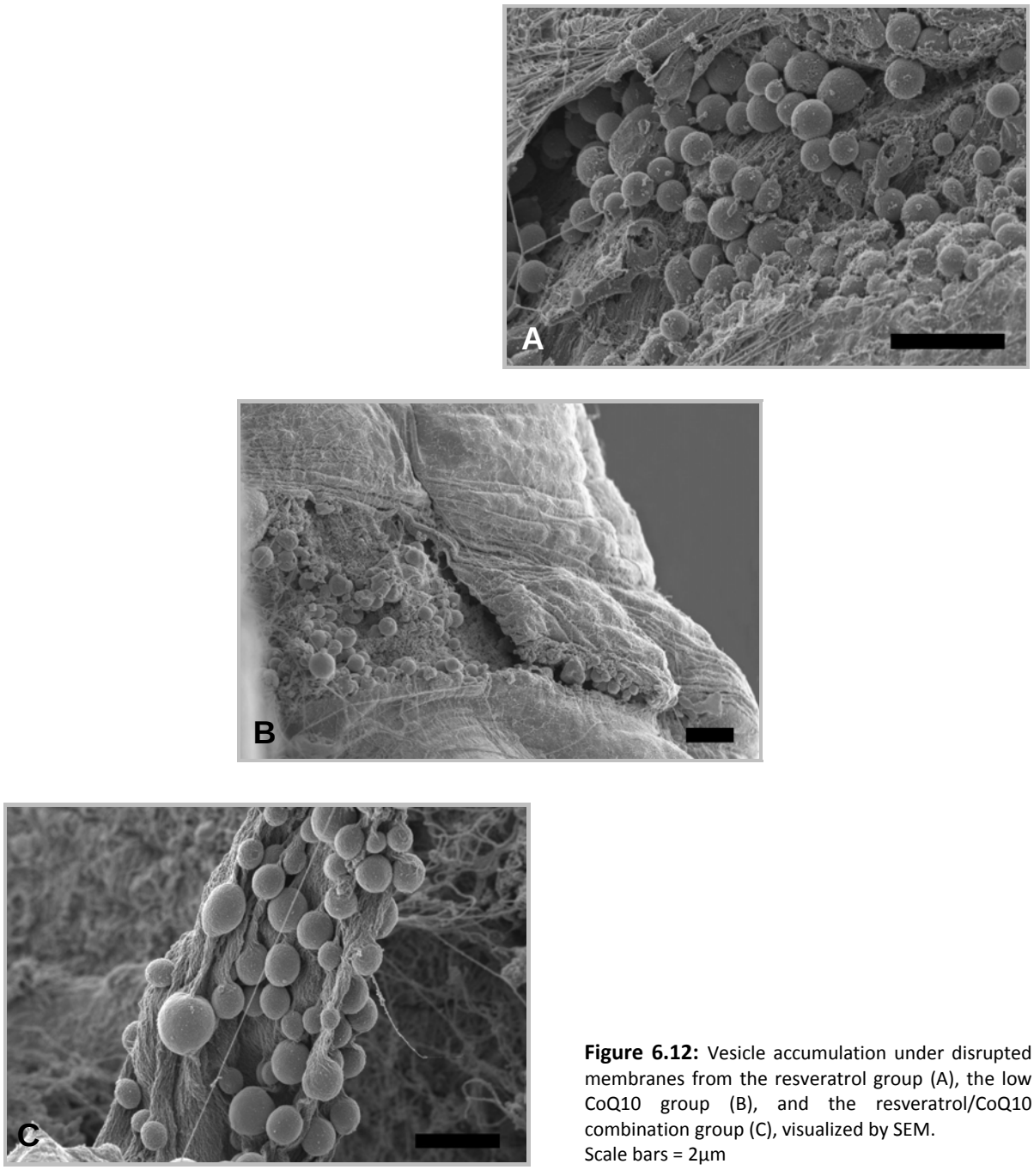

Figure 6.12: Vesicle accumulation under disrupted membranes from the resveratrol group (A), the low CoQ10 group (B), and the resveratrol/CoQ10 combination group (C), visualized by SEM.
Scale bars = 2µm

Other non-specific changes in the ultrastructure of SJL/J mice in the present study included, myofibrillar bending around an indentation in a muscle fiber (Figures 6.6, D and E; 6.7, E and 6.9 B), Z-disc streaming (Figure 6.7, D), and the formation of membranous whorls (Figure 6.9, F). The bending of the myofibrils around indentations in a muscle fiber created the impression of pressure exerted on the fiber *in vivo*. If this happens to be the reason, it is still not clear what caused the

pressure to the fiber, although one possibility might have been the invasion of fibers by inflammatory cells and their phagocytic activity (Figure 6.6 D). Alternatively and more likely, the muscles were in a contracting state when the animal was terminated and therefore, the sample was fixed in this state. SEM micrographs revealed a rippling effect in many fibers, in all groups, including muscle fibers from the negative control SWR/J mice. This proves that the event was not specific to the SJL/J mice, and thus not an alteration caused by the dystrophic process. In addition to the rippled fibers, normal fibers were also observed. Figure 6.11, C represents a micrograph of muscle fibers from the negative control group that did not display the rippling effect. It can therefore be suggested that the indentations observed in light microscopic images in chapter 5 and transmission electron micrographs in the present chapter, were present in the muscle before fixation.

Figure 6.13: Scanning electron micrographs of the indentations seen in transmission electron micrographs (present chapter) and light microscopy images (chapter 5). Micrograph (A) represents fibers from the negative control group, (B) represents fibers from the positive control group, and (C) represents a fiber from the high CoQ10 group. SEM clarified the uncertainty about the indentations; their formation occurred before fixation. Scale bars = 20µm

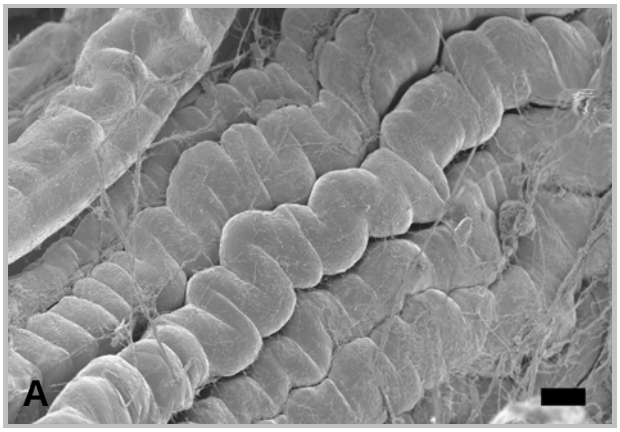

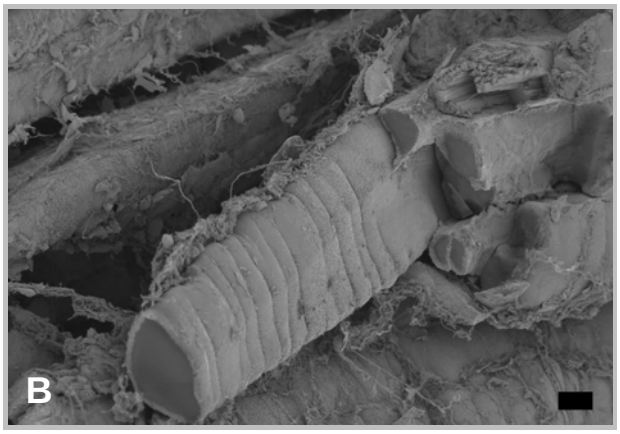

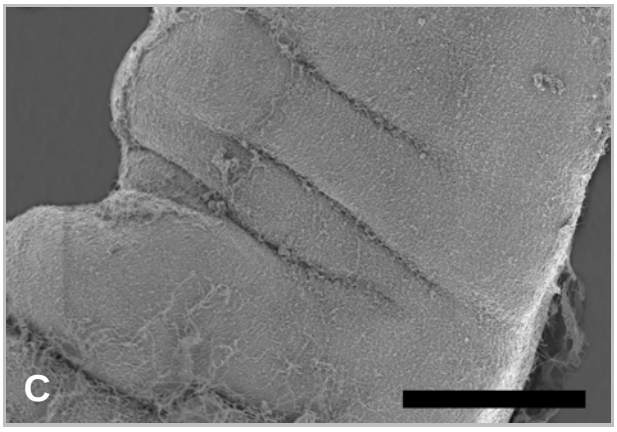

6.4 Concluding Remarks

Membrane repair requires efficient membrane fusion, a process that has been suggested by various lines of evidence, to involve dysferlin (Bansal *et al*., 2003; Selcen *et al*., 2001; De Luna *et al*., 2006; Klinge *et al*., 2007). Subsarcolemmal vesicle accumulation and vacuoles contiguous with the T-tubule system are two of the ultrastructural hallmarks of dysferlinopathy (Selcen *et al*., 2001; Cenacchi *et al*., 2005). The results from the qualitative ultrastructural analysis of quadriceps muscle from SJL/J dysferlin-deficient mice showed that vacuole formation occurred in muscle tissue of all groups of SJL/J mice as well as in the SWR/J mice. The results revealed that larger vacuoles were derived from mitochondrial degeneration. Also, large numbers of smaller vacuoles and vesicles presumably derived from the T-tubule system were observed in SJL/J mice, and vary in antioxidant supplemented groups.

Other non-specific changes observed, included Z-disc streaming, and the formation of membranous whorls. Although not attributable to the antioxidant supplementation or the lack thereof, this data provides concrete evidence for alternative non-specific changes in dysferlin-deficient muscle on the ultrastructural level in SJL/J mouse muscle.

Micrographs from the untreated positive control group in the present study revealed myofibrillar loss (Figure 6.4, A), while micrographs from the other groups, did not show this loss. Myofibrillar loss is best assessed on transverse sections (Carpenter and Karpati, 1984). The statement by Carpenter and Karpati, 1984, that far too many micrographs have been interpreted to indicate myofibril loss, while the myofibrils have just left the plane of sectioning, initiated utmost care when interpreting myofibrillar loss in the present study.

Qualitative ultrastructural analysis could not reliably discriminate between the myofibril condition of groups that have been treated with different antioxidants at different concentrations. The present chapter therefore, solely offered qualitative information on specific and non-specific alterations in dysferlin-deficient SJL/J quadriceps muscle. The study provides evidence for alterations to mitochondria on the ultrastructural level, consistent with ultrastructural changes found in mitochondria exposed to oxidative stress (Haycock *et al*., 1996). This data therefore suggests that muscle tissue in SJL/J mice are subjected to oxidative stress. This finding provided good reason for oxidative stress analysis in muscle tissue from SJL/J mice.

Ultrastructural analysis by TEM can be regarded a useful tool in investigating and identifying non-specific alterations in dysferlin-deficient muscle. Unfortunately, it does not clearly differentiate the possible effects of different antioxidant supplementations between different groups in the SJL/J

model using a limited sample size. In addition, ultrastructural analysis by SEM, did not nearly afford qualitative analysis of non-specific changes in SJL/J mouse muscle tissue to the extent that was afforded by TEM. Nevertheless, ultrastructural analysis utilizing SEM, provided clarity on the finding of muscle fiber indentations that was left unresolved by light microscopy and TEM. It further provided a true representation of the surface morphology of specific cell structures like vesicles, myofibrils and mitochondria.